The effect of Thole functions on the simulation of ionic liquids with point induced dipoles at various densities

Thomas Taylor, Michael Schmollngruber, Christian Schröder, and Othmar Steinhauser

Articles you may be interested in

Simulating polarizable molecular ionic liquids with Drude oscillators
The Journal of Chemical Physics **133**, 154511154511 (2010); 10.1063/1.3493689

On the collective network of ionic liquid/water mixtures. IV. Kinetic and rotational depolarization
The Journal of Chemical Physics **140**, 204505204505 (2014); 10.1063/1.4878116

The effect of Thole functions on the simulation of ionic liquids with point induced dipoles at various densities

Thomas Taylor, Michael Schmollngruber, Christian Schröder,[a] and Othmar Steinhauser
Department of Computational Biological Chemistry, University of Vienna, Währingerstrasse 17, A - 1090 Vienna, Austria

Point-induced dipoles are used to mimic electronic degrees of freedom in molecular dynamics simulations. Ultrashort distance interactions of these induced dipoles are damped by the so-called Thole functions to avoid the "polarization catastrophe." This study aims at the overall impact of Thole functions on structure as well as single-particle and collective dynamics of the ionic liquid 1-ethyl-3-methylimidazolium trifluoromethylsulfonate and thereby extends common studies of the effect of Thole functions on energy minimized geometries. © *2013 AIP Publishing LLC.*
[http://dx.doi.org/10.1063/1.4807093]

I. INTRODUCTION

The last decade has seen a diversity of classical molecular dynamics (MD) simulations of ionic liquids based on force fields with permanent charges.[1,2] In particular, imidazolium-based ionic liquids attracted the most computational interest since much experimental data exist. For example, the self-aggregation of alkyl side chains has been reported from x-ray experiments[3,4] and by MD simulations.[5–7] Urahata *et al.* confirmed the experimentally suggested preferred anion positions near the imidazolium ring as a function of the side chains.[8] The most prominent and successful force field of this era was proposed by Pádua and Canongia Lopes,[9,10] which is also the basis of this work.

Experience has shown that permanent charges alone create forces that are too directional: For example, the local structure of an imidazolium ring and the first CH_2-unit attached to the nitrogens is almost rigid. Consequently, the electrostatic potential of a central imidazolium i with fixed partial charges $q_{i\beta}$ produces a jagged energy surface of more or less deep valleys forcing surrounding ions in particular positions. Moreover, these energetic valleys are preserved when switching from one molecule i of a species to another, although the corresponding environments between the two molecules may differ significantly and, consequently, so may the local electric field around these molecules. As a result, these systems are too structured and their dynamics are retarded.[2,11–16] As a first remedy, several groups reduced the partial charges, resulting in a non-integer molecular charge of less than $\pm$ 1 e, making the energetic valleys more shallow and accelerating the dynamics.[17–25] However, the problem of the prefabricated favorable positions remains in these classical MD simulations.

This problem can be solved by transient reorganization of the molecular charge distribution. In principle, *ab initio* methods inherently include the electronic degrees of freedom and allow for a flexible charge distribution as a function of the local environment but these methods suffer from their ex-tremely high computational effort. As a result, the number of ion pairs is restricted to less than 100 and the trajectory period to less than a 100 ps.[40–43] Unfortunately, such small systems are prone to considerable size effects[44] and may not represent a liquid but an ionic cluster. However, techniques to mimic charge reorganization with acceptable numerical effort have been developed in the literature.[45] The most prominent examples are fluctuating charges,[46–48] Drude oscillators (charge on a spring model),[16,28,49–52] and point-induced dipoles (PID).[11,30–32,34–37] In principle, all these polarizable models are available in the standard MD package CHARMM,[29] but only the Drude oscillator model is currently supported. Unfortunately, the interaction between point-induced dipoles in CHARMM (c37b1) is simply cut beyond the cut-off radius. The standard MD packages GROMACS[53] and DL POLY[33] provide a Drude oscillator model for polarization, whereas AMBER[39] favors PID. Polarizable simulations of ionic liquids are usually on the basis of point-induced dipoles, as visible in Table I. Only our group uses Drude oscillators as well which are more common in protein force fields.

To our best knowledge, AMBER is the only prominent MD program offering several types of Thole functions to damp induced dipolar interaction at short distances.[54] In order to test this set, we will stick to AMBER in this work. Thereby, our goal is not to optimize the existing non-polar force field[9,10] for 1-ethyl-3-methylimidazolium (C_2mim^+) trifluoromethylsulfonate (TfO$^-$) by optimization of polarizabilities and a reparametrization of the Lennard-Jones parameter afterwards, but monitoring structural and dynamical changes using various Thole functions and standard polarizabilities.[55] To our best knowledge, this is the first study to investigate the effect of Thole functions during simulation and not from energy minimized structures.[54–57]

II. THEORY

A. Point-induced dipole model

The point-induced dipole method augments the standard set of coordinates $\{\mathbf{r}_\beta\}$ (representative of the nuclear

[a]Electronic mail: christian.schroeder@univie.ac.at

TABLE I. Overview of polarizable simulation in ionic liquids. The polarization forces can be treated either by a self-consistent field (SCF) or by a Lagrangian (LAG) approach.

Research group	Model	Minimization	MD
Schröder and Steinhauser[16, 26–28]	Drudes	LAG	CHARMM[29]
Voth and Knox[11, 30–32]	PID[a]	LAG	DL POLY[33]
Chang and Dang[34]	PID	SCF	
Borodin[35–37]	PID	SCF	LUCRETIUS[38]
This work	PID	LAG	AMBER[39]

[a]Although standard DL POLY does not offer a PID model, Voth and Knox seemed to have a self-contained version using PID.[31]

degrees of freedom) by a set of atomic dipoles $\{\boldsymbol{\mu}_\beta^{\mathrm{ind}}\}$ which are intended to represent the electronic degrees of freedom. Consequently, the potential energy of the classical force field $U^{\mathrm{nuc}}(\{\mathbf{r}_\beta\})$ is augmented by a polarizable contribution $U^{\mathrm{pol}}(\{\mathbf{r}_\beta\}, \{\boldsymbol{\mu}_\beta^{\mathrm{ind}}\})$,

$$U^{\mathrm{pol}}(\{\mathbf{r}_\beta\}, \{\boldsymbol{\mu}_\beta^{\mathrm{ind}}\}) = -\sum_\beta \boldsymbol{\mu}_\beta^{\mathrm{ind}} \cdot \mathbf{E}_\beta + \sum_\beta \sum_{\gamma \neq \beta} \boldsymbol{\mu}_\beta^{\mathrm{ind}} \mathbf{T} \boldsymbol{\mu}_\gamma^{\mathrm{ind}}$$
$$+ \frac{1}{2} \sum_\beta \frac{(\boldsymbol{\mu}_\beta^{\mathrm{ind}})^2}{\alpha_\beta}. \qquad (1)$$

Here, the dipole-dipole tensor $\mathbf{T}$ is a function of the distance $r = |\mathbf{r}_\beta - \mathbf{r}_\gamma| = \{x, y, z\}$ between the two interacting atoms (see Fig. 1). $U^{\mathrm{nuc}}(\{\mathbf{r}_\beta\})$ comprises all bonded and non-bonded terms of a classical force field. In particular, it contains the interaction U^{elec} between the permanent charges q_β. Its derivative determines the electrostatic field $\mathbf{E}_\beta = -\nabla_\beta U^{\mathrm{elec}}/q_\beta$ at the position of the atom β and couples the nuclear and electronic degrees of freedom.

In the spirit of the Born-Oppenheimer approximation, the complete potential energy $U^{\mathrm{tot}}(\{\mathbf{r}_\beta\}; \{\boldsymbol{\mu}_\beta^{\mathrm{ind}}\}) = U^{\mathrm{nuc}}(\{\mathbf{r}_\beta\}) + U^{\mathrm{pol}}(\{\mathbf{r}_\beta\}, \{\boldsymbol{\mu}_\beta^{\mathrm{ind}}\})$ is minimized with respect to the electronic degrees of freedom represented by the point dipoles $\{\boldsymbol{\mu}_\beta^{\mathrm{ind}}\}$, while nuclear degrees of freedom $\{\mathbf{r}_\beta\}$ are kept fixed, i.e., $U^{\mathrm{nuc}}(\{\mathbf{r}_\beta\})$ is constant during the minimization process. This leads to the minimum condition

$$\boldsymbol{\mu}_\beta^{\mathrm{ind}} - \alpha_\beta \left(\mathbf{E}_\beta - \sum_\gamma^N \mathbf{T} \boldsymbol{\mu}_\gamma^{\mathrm{ind}} \right) = 0, \qquad (2)$$
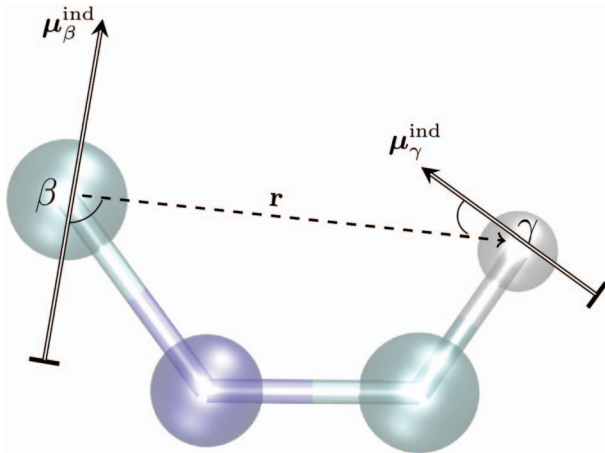

FIG. 1. Interaction between two induced dipoles.

and can easily be rewritten in a matrix representation,

$$\begin{pmatrix} \alpha_1^{-1} & \mathbf{T}_{12} & \cdots & \mathbf{T}_{1N} \\ \mathbf{T}_{12} & \alpha_2^{-1} & \cdots & \mathbf{T}_{2N} \\ \vdots & & \ddots & \\ \mathbf{T}_{N1} & \mathbf{T}_{N2} & \cdots & \alpha_N^{-1} \end{pmatrix} \begin{pmatrix} \boldsymbol{\mu}_1^{\mathrm{ind}} \\ \boldsymbol{\mu}_2^{\mathrm{ind}} \\ \vdots \\ \boldsymbol{\mu}_N^{\mathrm{ind}} \end{pmatrix} = \begin{pmatrix} \mathbf{E}_1 \\ \mathbf{E}_2 \\ \vdots \\ \mathbf{E}_N \end{pmatrix}. \qquad (3)$$

In principle, the induced dipoles can be obtained from the last equation by matrix inversion, but due to the high number of degrees of freedom an iterative approach is usually chosen, i.e., the induced dipoles $\boldsymbol{\mu}_\beta^{\mathrm{ind}}$ in Eq. (2) are subsequently used to compute the induced dipole moments for the other atoms. This procedure is repeated until the induced dipole moments do not change anymore. If the threshold is sufficiently small, one gets close enough to the potential minimum of energy $U_{\mathrm{min}}^{\mathrm{pol}}$,

$$U_{\mathrm{min}}^{\mathrm{pol}} = -\frac{1}{2} \sum_\beta \boldsymbol{\mu}_\beta^{\mathrm{ind}} \cdot \mathbf{E}_\beta, \qquad (4)$$

which represents half of the interaction energy between nuclear and electronic degrees of freedom. In other words, at the minimum, the mutual coupling of induced dipoles augmented by their self-energy exactly compensates one half of the interaction energy in Eq. (1).

The dipole-dipole tensor $\mathbf{T}$ is the central quantity of the coupling of induced dipole moments sketched in Fig. 1. It is the negative double-gradient $\mathbf{T} = -\nabla\nabla\phi_k(r)$ of the respective modified Coulomb interaction $\phi_k(r)$,

$$\mathbf{T} = -\frac{1}{r} \frac{d\phi_k}{dr} \mathbf{I} \quad -\frac{1}{r^2} \left(\frac{d^2\phi_k}{dr^2} - \frac{1}{r} \frac{d\phi_k}{dr} \right) \mathbf{r} : \mathbf{r} \qquad (5)$$

$$= f_1(\phi_k, r) \mathbf{I} - f_2(\phi_k, r) \mathbf{r} : \mathbf{r}, \qquad (6)$$

with $\mathbf{r} : \mathbf{r}$ being the dyadic product of the bond vector. Since $\mathbf{I}$ represents a unity matrix, the first part of $\mathbf{T}$ depends solely on the distance r between the interacting atoms β and γ. Consequently, this part of the dipole-dipole tensor correlates the mutual orientation of the interacting dipoles

$$\boldsymbol{\mu}_\beta^{\mathrm{ind}} \mathbf{T} \boldsymbol{\mu}_\gamma^{\mathrm{ind}} = f_1(\phi_k, r) \boldsymbol{\mu}_\beta^{\mathrm{ind}} \cdot \boldsymbol{\mu}_\gamma^{\mathrm{ind}}$$
$$- f_2(\phi_k, r) (\boldsymbol{\mu}_\beta^{\mathrm{ind}} \cdot \mathbf{r})(\boldsymbol{\mu}_\gamma^{\mathrm{ind}} \cdot \mathbf{r}). \qquad (7)$$

If the induced dipoles $\boldsymbol{\mu}_\beta^{\mathrm{ind}}$ and $\boldsymbol{\mu}_\gamma^{\mathrm{ind}}$ are perpendicular to each other, $f_1(\phi_k, r)$ becomes meaningless for the dipolar interaction. In contrast, if both induced dipole moments are parallel to each other, $f_1(\phi_k, r)$ has the maximum effect. The second part of $\mathbf{T}$ contains information on the mutual position of the interacting atoms. Hence, this part of the dipole-dipole tensor correlates the induced dipoles with the bond vector $\mathbf{r}$ connecting these dipoles. This is indicated by the arcs in Fig. 1. If one of induced dipoles is almost perpendicular to the connecting vector $\mathbf{r}$ (e.g., $\boldsymbol{\mu}_\beta^{\mathrm{ind}}$ and $\mathbf{r}$ in Fig. 1), $f_2(\phi_k, r)$ gets irrelevant. However, if both dipoles are on top of each other, i.e., both are parallel to $\mathbf{r}$, $f_2(\phi_k, r)$ reaches its maximum importance.

TABLE II. Various Thole screening functions. For further details see Ref. 54.

Thole function	Shape function	Default Thole radius R
ϕ_0 (Coulomb)	$\frac{d\phi_0}{dr} = -\frac{1}{r^2}$	
ϕ_1 ("linear")	$\frac{d\phi_1}{dr} = -\frac{1}{r^2}\begin{cases}1 & r \geq R \\ 4\left(\frac{r}{R}\right)^3 - 3\left(\frac{r}{R}\right)^4 & r < R\end{cases}$	$1.662\,(\alpha_\beta \cdot \alpha_\gamma)^{\frac{1}{6}}$
ϕ_2 (exponential)	$\frac{d\phi_2}{dr} = -\frac{1}{r^2}\left(1 - e^{-Rr^3}\right)$	$0.572\,(\alpha_\beta \cdot \alpha_\gamma)^{-\frac{1}{2}}$
ϕ_3 (exponential)	$\frac{d\phi_3}{dr} = -\frac{1}{r^2}\left(1 - e^{-Rr}\left(\frac{1}{2}R^2\,r^2 + R\,r + 1\right)\right)$	$2.089\,(\alpha_\beta \cdot \alpha_\gamma)^{-\frac{1}{6}}$

B. Thole functions

In the original point-induced dipole model by Applequist,[58] the Coulomb potential ϕ_0 is unmodified, i.e., $\phi_0 = r^{-1}$. This model reproduced mean polarizabilities satisfactorily but overestimated the anisotropy of the polarizability.[54] Furthermore, at short distances the interaction of the induced dipoles becomes too strong leading to even shorter distances and consequently stronger interactions. This so-called "polarization catastrophe" also manifests in the ill-condition of the matrix on the left-hand side of Eq. (3). For small distances r, the values of the $\mathbf{T}_{\beta\gamma}$-submatrices are in the same order of magnitude as the inverse values of the polarizability. As a result, the inverse of the matrix in Eq. (3) may not be positive definite anymore leading to negative eigenvalues, i.e., induced dipoles pointing in the opposite direction of the underlying electric field.[54] In order to avoid such unphysical effects, Thole has suggested several inner damping functions ϕ_k of the Coulomb interaction (see Table II) affecting the corresponding dipole-dipole tensor $\mathbf{T}$.

FIG. 2. Dipolar interaction modified by Thole functions ϕ_k. Please note that both axes are dimensionless.

The effect of the linear (blue) and exponential (orange and red line) damping functions is demonstrated in Fig. 2. The idea behind these damping functions is that the modified $\mathbf{T}$-tensor should still be able to keep its tensoric character, i.e., it should be invariant to the rotation or translation of the coordinate system. As a consequence, the modified $\mathbf{T}$-tensor still fulfills Eq. (5). Additionally, the damping function should be scalable from microscopic to macroscopic polarizabilities and distances.[54] Therefore, the distance in the shape functions $d\phi_k/dr$ is always divided by a corresponding Thole "radius" R (see Table II). This radius consists of the respective polarizabilities in order to get dimensionless properties and a prefactor which was determined by a fitting procedure to experimental polarizabilities.[54] This way, the overestimated anisotropy of the pure Applequist model could be avoided.[54,55] Moreover, the shape functions ϕ_k and their derivative reduce the respective $\mathbf{T}$-tensors at short distances. This way, the off-diagonal contributions of the matrix in Eq. (3) become less critical, making diagonal elements more prominent.

Figure 2 demonstrates the consequences of the Thole damping model. In the case of parallel dipoles which are perpendicular to the bond vector r (see Fig. 2(a)), only $f_1(\phi_k, r)$ affects the damping, i.e., the shape functions divided by the distance r. Here, the infinite value of $\phi_0(r \to 0)$ is reduced to a small non-zero value depending on the respective ϕ_k. This weakening of the dipolar interaction at short distances is sufficient to avoid the "polarization catastrophe." In the case of perpendicular induced dipoles, only $f_2(\phi_k, r)$ plays a role. In Fig. 2(b), the negative half of $f_2(\phi_k, r)$ is displayed because of the angle of $\pi/4$ and $3/4\,\pi$ between the dipoles and the bond vector, respectively. However, at short distances, the dipolar interaction is reduced to zero by the Thole functions. In Fig. 2, the "intramolecular regime" is indicated by vertical lines. It comprises typical distances between atoms connected by a harmonic bond or an angle potential. The shortest possible intermolecular distances can be found for hydrogen bonds. This zone starts at approximately $2.5(\alpha_\beta \cdot \alpha_\gamma)^{1/6}$. The polarizability scaling factor $(\alpha_\beta \cdot \alpha_\gamma)^{1/6}$ ranges from 0.75 Å, e.g., between two hydrogen or a hydrogen and a fluorine, to 1.1 Å in case of two carbons or a sulfur/oxygen interaction.[55]

III. METHODS

The molecular dynamics simulations of [C$_2$mim][TfO] were carried out with AMBER 11 (see Ref. 39) on a Sun Fire X2270 dual Quadcore (Intel X5550, 2.66 GHz) using 32
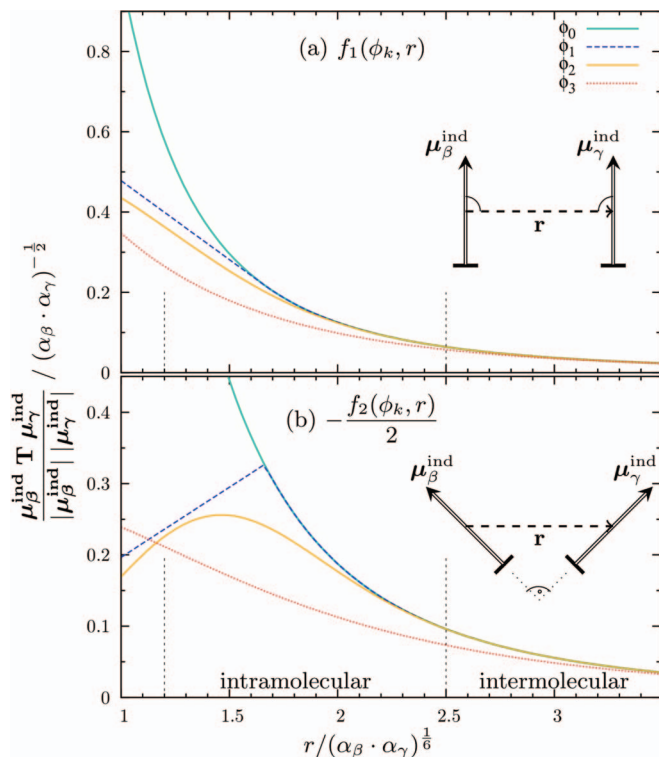
TABLE III. Computational effort of various MD methods to produce a 100 ps trajectory slice of 1000 ionic liquid ion pairs.

Model	Method	Stringency	CPU time (h)
Non-polarizable			1.4
PID	LAG	$T_\mu = 40.0\,\mathrm{K}$	2.2
PID	LAG	$T_\mu = 0.06\,\mathrm{K}$	2.0
Drudes[16]	LAG	$T_\mu = 1\,\mathrm{K}$	2.7
PID	SCF	$\delta\mu \le 10^{-4}\,\mathrm{D}$	3.9
PID	SCF	$\delta\mu \le 10^{-7}\,\mathrm{D}$	25.0

computer cores per job. Since we have shown in a recent paper[44] that 500 ion pairs are the minimum system size to compute reliable dynamics of an ionic liquid system, our simulation box contains $N = 1000$ ion pairs to be on the safe side. This corresponds to 27 000 atoms. In order to cope with the long range nature of Coulomb interactions in a finite system, all simulations were carried out with an Ewald κ of 0.41 Å^{-1}, a skin of 2.0 Å, and a van-der-Waals cut-off of 10.0 Å. The temperature was adjusted to 300 K by a Berendsen thermostat and trajectories are computed for at least 15 ns and extend up to 30 ns.

In principle, polarizable simulations are more CPU time consuming than non-polarizable ones, but the combination of point-induced dipoles and Lagrangian thermostats enables us to confine the additional effort to 40% as shown in Table III. This is faster than our previous Drude model which expanded the numerical effort by a factor of 1.9. The table also shows that the increased accuracy ($T_\mu = 0.06$ K) of the Lagrangian methods does not result in a significant increase in computational time. However, the dynamics is accelerated by approximately 10% since the more optimized induced dipoles ($T_\mu = 0.06$ K) shield the adhesive interaction between cations and anions better as compared to the weak Lagrangian thermostat with an average temperature of $T_\mu = 40$ K for the induced dipole motion.

In contrast, conventional self-consistent field (SCF) approaches are slower by a factor of at least 3 for very low accuracy ($\delta\mu \le 10^{-4}$D) or 18 at standard accuracy of $\delta\mu \le 10^{-7}$D. In these cases, the SCF iteration is stopped at step n, if the changes of induced dipoles,

$$\delta\mu(n) = \sqrt{\frac{\sum_\beta^N (\boldsymbol{\mu}_\beta(n) - \boldsymbol{\mu}_\beta(n-1))^2}{N}} \qquad (8)$$

have become numerically negligible. Unfortunately, a slack SCF-threshold of $\delta\mu \le 10^{-4}$D means that the potential minimum of U_{min}^{pol} in Eq. (4) is not reached. This leads to an artificial deceleration of dynamics which is worse than the effect of a Lagrangian thermostat T_μ of 40 K.

AMBER 11 was used together with version 1.5 of AmberTools.[39] The latter is of importance since our Drude force field[16] including polarizabilities of van Duijnen[55] and classical force field parameters of Pádua and Canongia Lopes[9, 10] was developed for CHARMM[29] and automatically translated for AMBER via CHAMBER. This ensures that the complete setup (including the accuracy of natural constants of

CHARMM) stays the same. Afterwards, hydrogen polarizabilities are added since they were not part of the above mentioned force field.[16] The polarizabilities of the non-hydrogen atoms are identical.

In order to elucidate the influence of the Thole damping in more detail, we started four independent simulations including the Thole functions $\phi_0-\phi_3$. These simulations were accompanied by a non-polarizable system. Furthermore, these simulations were performed at two different densities, $\rho_{exp} = 1.384$ and $\rho_{ff} = 1.437$ g/cm³. The corresponding box lengths are 67.8 Å and 67.0 Å, respectively. The lower density corresponds to the experimental value,[59] while the higher density is obtained by a NPT equilibrium simulation prior to the production runs. This discrepancy of 3.8% between the experimental and the force field density is already found for the non-polarizable force field.[10] In contrast, Borodin reported that turning off the cationic polarizability results in a density decrease of 0.8% in case [C$_2$min][BF$_4$], whereas anionic polarizability seems to have no influence on density.[35]

IV. RESULTS AND DISCUSSION

A. The influence of density on the structure and dynamics

At first sight, one would expect that increasing the density would lead to a more or less uniform reduction of the interionic distances. However, in practice, it turns out that the increasing density primarily affects distances between ions of the same charge. As visible in Fig. 3(a), the center-of-mass distances between the cations and anions is unaffected by the increase in density. This is true for the non-polarizable (gray and black) as well for the polarizable (bright and dark green)
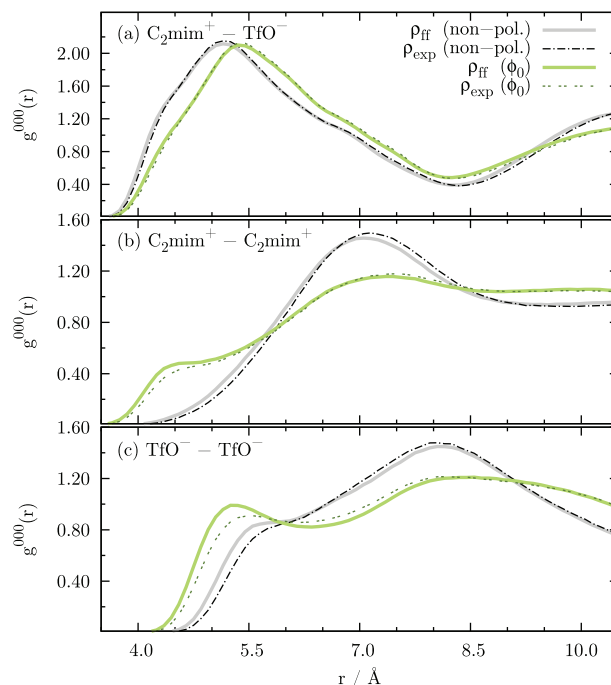

FIG. 3. Change of the radial distribution functions as a function of polarizability and density.

TABLE IV. System dynamics as a function of density ρ and Thole screening function ϕ_k.

		Structure			Rotation				Translation					
Method	ρ (g/cm^3)	ϕ_k	G_K^{++}	G_K^{--}	G_K^{+-}	$\langle\tau_{\text{ind}}^+\rangle$ (ns)	$\langle\tau_{\text{ind}}^-\rangle$ (ns)	$\langle\tau_{\text{rot}}^+\rangle$ (ns)	$\langle\tau_{\text{rot}}^-\rangle$ (ns)	D^+ (10^{-8}cm^2/s)	D^- (10^{-8}cm^2/s)	$\langle\tau_{\text{cage}}^{++}\rangle$ (ns)	$\langle\tau_{\text{cage}}^{--}\rangle$ (ns)	$\langle\tau_{\text{cage}}^{+-}\rangle$ (ns)	$\sigma(0)$ (S/m)
Non-pol.	1.437		0.71	0.67	1.17			7.3	2.1	1.9	0.87	≈72	≈83	≈92	0.052
LAG	1.437	ϕ_0	0.78	0.88	0.94	0.29	0.32	1.3	0.35	13.4	9.4	7.7	7.2	8.8	0.33
LAG	1.437	ϕ_1	0.97	0.88	0.94	0.29	0.31	1.3	0.34	13.1	9.4	8.0	7.6	9.1	0.29
LAG	1.437	ϕ_2	0.97	0.88	0.95	0.24	0.28	1.2	0.26	14.8	9.4	7.4	7.7	8.8	0.36
LAG	1.437	ϕ_3	0.99	0.86	0.96	0.33	0.39	1.5	0.40	11.1	6.7	11	12	14	0.29
Non-pol.	1.384		0.96	0.86	1.17			2.5	0.59	5.6	1.8	≈23	≈25	≈38	0.22
LAG	1.384	ϕ_0	0.98	0.88	0.93	0.11	0.12	0.43	0.13	34.7	24.6	2.9	2.7	4.6	0.77
LAG	1.384	ϕ_1	1.01	0.88	0.95	0.12	0.12	0.44	0.13	34.3	23.7	3.0	2.9	4.7	0.64
LAG	1.384	ϕ_2	0.98	0.87	0.95	0.10	0.12	0.40	0.12	38.6	23.2	2.8	2.9	4.6	0.88
LAG	1.384	ϕ_3	0.97	0.85	0.96	0.11	0.13	0.49	0.15	34.0	20.8	3.8	3.8	5.5	0.75

simulations. However, the probability for hydrogen-bonding of the imidazolium hydrogens is slightly affected. The chance to find a hydrogen bond[60] of an imidazolium ring hydrogen to a triflate fluorine in the non-polarizable simulations is approximately 10% and 9% for ρ_{ff} and ρ_{exp}, respectively. These chances are scaled roughly by a factor of 0.9 in case of the polarizable force field. Additionally, 2% of the imidazolium ring hydrogens are hydrogen-bonded to triflate oxygens, irrespective of the density and polarizability. The center-of-mass distances of adjacent cations is shifted by a little bit more than 2% in Fig. 3(b). The density effect on the anions is even stronger (see Fig. 3(c)). Nevertheless, the overall shape of the radial distribution functions including peaks and shoulders is conserved in all cases.

However, the effect of polarizability is enormous at both densities. The induced dipoles act as an "inner solvent" reducing the effective charge of the molecules.[28,61] Consequently, the attractive interaction between cations and anions is reduced and the center-of-mass distance is shifted by 0.5 Å in the first shell. In contrast, the distance between the centers-of-mass of adjacent cations is reduced due to the lower charge repulsion. The emerging shoulder at 4.4 Å in case of the polarizable systems can be attributed to π-stacked imidazolium rings and was also observed in case of [C$_2$mim][NO$_3$].[31] The lower charge repulsion due to the shielding by the polarizability is also visible in the radial distribution functions between anions. Since the charge density at the surface of the anions is higher when compared to the bulkier cations, the polarizability effect is stronger.

In case of [C$_2$mim][NO$_3$], Yan *et al.* also reported a reduced Coulombic repulsion between like ions due to the induced dipoles,[31] but the impact is smaller than reported here. This may be due to the higher temperature of their simulations (=400 K) and/or their lower polarizabilities, i.e., α(C$_2$mim) is 11.8 Å^3 and 14.2 Å^3 for their and our simulations, respectively. However, the reduction of Coulombic interactions by induced dipoles is also known for molten salts.[62]

The radial distribution function $g^{000}(r)$ probes the distance between the molecules. Their orientation can be measured by the orientational correlation function $g^{110}(r)$ for cations–anions, cations–cations, and anions–anions.[63] These distance-dependent functions can be integrated to yield the so-called Kirkwood G_K-factor,[63]

$$G_K = 1 + 4\pi\rho \int_0^{"\infty"} g^{110}(r)\, r^2 dr. \tag{9}$$

The corresponding values for our (non-)polarizable [C$_2$mim][TfO]-systems under investigation are given in Table IV. Interestingly, the Kirkwood-factor G_K^{+-} for the non-polarizable systems is 1.17 at both densities indicating a weak preference for parallel dipoles between cations and anions. However, the point-induced dipoles weaken the correlation between cations and anions and the parallel dipolar alignment vanishes. The dipolar alignment for cation–cation and anion–anion depends on the density. At ρ_{exp} = 1.384 g/cm^3, the system seems to be more relaxed compared to the higher density. Consequently, the dipolar orientation and hence G_K^{++} and G_K^{--} do not change when switching on the polarizability. In contrast, the anions at ρ_{ff} = 1.437 g/cm^3 seem to be so close to each other that the unhindered charge repulsion forces orient the anionic dipoles in an antiparallel way (G_K^{--} = 0.67). The point-induced dipoles extenuate the charge repulsion and weaken the preference for antiparallel anionic dipoles. In case of the cations, the polarizable effect is weaker but present.

In agreement with Ref. 31, the structural oscillations in $g^{000}(r)$ extend over more than 20 Å at both densities indicating strong long-range forces which should be of electrostatic nature. These oscillations are even more prominent in the non-polarizable systems and can be detected up to 40 Å.

The higher value of the density in the MD simulations can also be reached in experiment by lowering the temperature by more than 30 K.[64] Of course, this temperature reduction goes along with an increase in viscosity and might be a reason for the slow dynamics of the Pádua force field.[9,10] It seems that the Lennard-Jones parameters used here (originally taken from the OPLS force field[65]) favor supercooling of the ionic liquid and should be optimized in future force fields. However, the dynamics can be accelerated in the MD simulation by a factor of approximately 2.7 when switching to the experimental density (ρ_{exp} = 1.384 g/cm^{-3}) as visible in Table IV. Interestingly, this acceleration factor applies to the translation motion, e.g., diffusion coefficients of the cations

and anions, as well as to the rotation, i.e., the relaxation constants for the induced and total dipole moments of the cations and anions. This uniform scaling points out that the underlying effect should have hydrodynamic character, i.e., the viscosities of the systems should differ by the acceleration factor.

However, we are interested in the effect of the Thole functions on the interaction between cations and anions of the ionic liquid in this work. Since effects should be more visible for the higher density, $\rho_{\text{ff}} = 1.437$ g/cm^{-3}, which corresponds to overall smaller distances between the ions (at least for like charges), we will use this system as reference for our observations. In addition, this is also the density at which the force field is in equilibrium.

B. Structural changes due to various Thole functions

The radial distribution functions $g^{000}(r)$ at force field density are depicted in Figs. 4(a)–4(c) with the effective Thole functions ϕ_k. Interestingly, the "linear" Thole function (ϕ_1, blue line) seems to have no specific effect on the structure of the ionic liquid since it yields the very same results as using no Thole function (ϕ_0, turquoise solid line) at all. The corresponding g-functions of both exponential Thole functions (ϕ_2, orange solid line) and (ϕ_3, red dashed line) differ significantly from those of ϕ_0 and ϕ_1 but are very similar to each other. First, the radial distribution function between cations shows a shoulder at 4.5 Å which is not present in case of the exponential Thole functions. At these short center-of-mass distances, this peak can be attributed to π-stacking imidazolium ring. In addition, the radial distribution function between the anions (see Fig. 4(c)) seems to be shifted outwards by 0.2 Å. In contrast, $g^{000}(r)$ between cations and anions is shifted inwards by 0.2 Å.

Overall, this can be explained by the lower molecular polarizability in case of exponential Thole functions. Inspecting Figs. 2(a) and 2(b) shows that the intramolecular dipole-dipole interaction is unaffected in case of ϕ_1 at distances between 1.5 and $1.9(\alpha_\beta \cdot \alpha_\gamma)^{1/6}$ but is screened for ϕ_2 and ϕ_3. Consequently, the inner solvent in case of ϕ_2 and ϕ_3 damps the repulsive interaction between like-charged ions less and therefore, too narrow positions seem unfavorable. This effect was already observed (even much stronger) for the juxtaposition of polarizable and non-polarizable simulations in Fig. 3.

Although emerging from atomic contributions, $\boldsymbol{\mu}_\beta^{\text{ind}} \mathbf{T} \boldsymbol{\mu}_\gamma^{\text{ind}}$, we interpret our data on a molecular level for the sake of simplicity and tradition. The molecular dipole μ_i consists of all permanent and induced contributions from all atoms β and γ. In particular, the induced contributions play an important role for the cationic dipoles. The dipole-dipole tensor $\mathbf{T}$ is not only affected by the distance of the two interacting dipoles but also by their orientation and position (see Fig. 2). Its influence on the molecular structure can be described by the orientational correlation functions $g^{110}(r)$ and $g^{101}(r)$ which are an extension to the radial distribution function $g^{000}(r)$,[63, 66]

$$g^{000}(r) = \frac{1}{\rho \cdot 4\pi r^2 dr} \left\langle \sum_j \delta(r - |\mathbf{r}_{ij}|) \right\rangle_i, \quad (10)$$

$$g^{110}(r) = \frac{1}{\rho \cdot 4\pi r^2 dr} \left\langle \sum_j \frac{\boldsymbol{\mu}_i \cdot \boldsymbol{\mu}_j}{|\boldsymbol{\mu}_i| \, |\boldsymbol{\mu}_j|} \delta(r - |\mathbf{r}_{ij}|) \right\rangle_i, \quad (11)$$

$$g^{101}(r) = \frac{1}{\rho \cdot 4\pi r^2 dr} \left\langle \sum_j \frac{\boldsymbol{\mu}_i \cdot \mathbf{r}_{ij}}{|\boldsymbol{\mu}_i| \, |\mathbf{r}_{ij}|} \delta(r - |\mathbf{r}_{ij}|) \right\rangle_i. \quad (12)$$
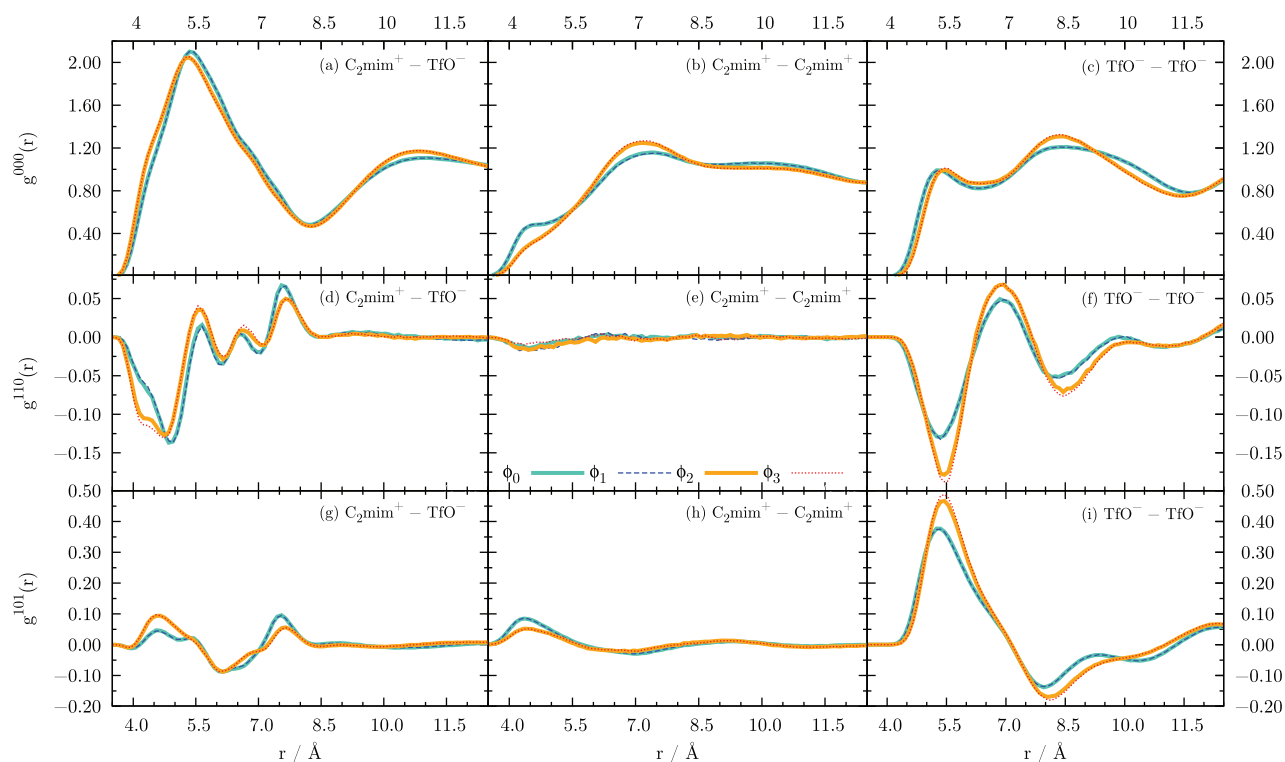

FIG. 4. Radial distribution and orientational correlation functions at ρ_{ff} for various Thole functions.

Here, the mutual orientation and position of the pair of dipoles $\boldsymbol{\mu}_i$ and $\boldsymbol{\mu}_j$ is reflected by $g^{110}(r)$ and $g^{101}(r)$, respectively.

Application of ϕ_0 and ϕ_1 results in an almost identical orientation of the ionic dipoles. The same holds true for the pair ϕ_2 and ϕ_3. However, the respective orientation of the second pair is more pronounced, in particular for the anion–anion correlation in Fig. 4(f). The orientational correlation function $g^{110}(r)$ indicates a preferred antiparallel alignment of dipoles between adjacent anions (see Fig. 4(f)) as well as between anions and cations (see Fig. 4(d)) because of the negative values at distances shorter than 6 Å. The overall alignment of anionic dipoles is also antiparallel as demonstrated by the corresponding G_K^{--} factor computed by Eq. (9). The collective cation-anion dipole alignment is weaker since the corresponding G_K^{+-} in Table IV approaches unity. Both, the $g^{110}(r)$-function in Fig. 4(e) and its corresponding integral over spherical shells G_K^{++} in Table IV show no systematic self-alignment of cationic dipoles.

$g^{101}(r)$ measures the anisotropy of ion distribution around a reference ionic dipole: Positive values indicate an ionic position in the northern hemisphere, whereas negative values refer to the southern region. For example, in case of a TfO$^-$ reference dipole, the northern hemisphere is around the CF$_3$-moiety. Correspondingly, for distances shorter than 6 Å Fig. 4(i) shows a crowding of TfO$^-$-ions around the CF$_3$-unit with antiparallelly aligned dipoles (see Fig. 4(f)). For larger distances the mutual dipolar orientation is reversed. The $g^{101}(r)$-functions involving the cation are rather flat, which would suggest an isotropic distribution. However, this is mainly caused by the large fluctuations of the reference cationic dipole. In addition, anions are usually located quite near the H2-hydrogen of the imidazolium ring. This configuration corresponds to an angle of a little less than 90° between $\mathbf{r}_{ij}$ and $\boldsymbol{\mu}_i$ and hence very small $g^{101}(r)$-values at distances shorter than 6 Å. As already observed for $g^{000}(r)$ and $g^{110}(r)$, the influence of the Thole functions again shows the resemblence of $\{\phi_0, \phi_1\}$ on the one side and $\{\phi_2, \phi_3\}$ on the other. Quite generally, the root of this pairing pattern is $g^{000}(r)$, which can in principle be shown by the normalized functions $g^{110}(r)/g^{000}(r)$ and $g^{101}(r)/g^{000}(r)$ (data not shown). This is also reflected by the Kirkwood-factors which are almost independent of the Thole function ϕ_k (see Table IV). This means that Thole damping is too weak to change the orientation and position of dipoles, it rather affects the translational packing of the ions. Considering non-polarizable and unchanged polarizable (ϕ_0) simulations, the exponential Thole functions, ϕ_2 and ϕ_3, seem to decrease the overall polarizability of the system by a small amount. In this way, Thole damping shifts the orientational structure a little towards that of the non-polarizable system.

C. The influence of Thole functions on the dynamics

The higher effective polarizability of ϕ_0 and ϕ_1 simulations is also reflected by the auto-correlation function of the induced dipole moments $\langle \boldsymbol{\mu}^{\mathrm{ind}}(0) \cdot \boldsymbol{\mu}^{\mathrm{ind}}(t) \rangle$. In order to be compatible with the dielectric spectrum discussed later we give N times the scaled Fourier Laplace transform,

$$\mathcal{L}_{\mathrm{V}}[f(t)] = \frac{1}{3V k_B T \epsilon_0} \int\limits_0^\infty -\frac{d}{dt} \langle f(0) \cdot f(t) \rangle \, e^{i\omega t} dt \quad (13)$$

in Figs. 5(a) and 5(b). Here, we find the pairing of $\{\phi_0, \phi_1\}$ and $\{\phi_2, \phi_3\}$ again. The higher effective polarizability of the systems affected by the Thole functions ϕ_0 and ϕ_1 can be deduced from the peak heights. The average relaxation constant $\langle \tau^{\mathrm{ind}} \rangle$ is given in Table IV for each Thole function, density, and species.

As the overall molecular polarizability of the cations is almost twice that of the anions, the corresponding peaks differ approximately by a factor of four. In contrast, this ratio of dipoles is reversed in case of molecular dipoles, comprising permanent and induced contributions. In case of the cations, induced dipoles contribute significantly ($\simeq 20\%$) to the molecular dipole spectrum given in Fig. 5(c). Since the permanent anionic dipoles are much stronger than their induced counterparts, they make up the anionic dipolar spectrum in Fig. 5(d). So far, we have only considered molecular spectra lacking any cross-correlations between the dipolar ions. However, the dominance of the permanent dipoles of the anions even produces an apparent similarity of the anionic molecular spectrum to the dielectric permittivity $\epsilon(\omega) = \mathcal{L}_{\mathrm{V}}[\mathbf{M}_{\mathrm{D}}(t)]$ governed by the overall collective rotational dipole moment $\mathbf{M}_{\mathrm{D}}(t)$. This similarity may be explained by the close-to-unity values of the three Kirkwood-factors G_K^{+-}, G_K^{--}, and G_K^{++} given in Table IV. At the collective level, the pairings $\{\phi_0, \phi_1\}$ and $\{\phi_2, \phi_3\}$ are not visible anymore since collective dielectric properties are of long-range nature and therefore involves those intermolecular distances where the Thole damping has leveled off.

Since the molecular ions C$_2$mim$^+$ and TfO$^-$ are not only dipolar but also charged species, the dielectric spectrum is enriched by translational contributions. Here, the volume expansion of the charge centers may be seen as additional intermolecular dipoles. Consequently, the translation of these charge centers governs the relaxation of the collective translational dipole moment $\mathbf{M}_{\mathrm{J}}(t)$. In principle, the translational contribution to the generalized dielectric constant can be obtained by $\vartheta(\omega) = \mathcal{L}_{\mathrm{V}}[\mathbf{M}_{\mathrm{J}}(t)]$, but in practice it is much easier to fit the initial region of the collective charge displacement $\langle \Delta \mathbf{M}_{\mathrm{J}}^2(t) \rangle$.[26,67] The curve presented in Fig. 5(f) was obtained by a fit of $\langle \Delta \mathbf{M}_{\mathrm{J}}^2(t) \rangle$ up to 500 ps although computed over the complete time window of the 30 ns trajectories.

As visible in Figs. 5(e) and 5(f), the dielectric permittivity $\epsilon(\omega)$ and the dielectric conductivity $\vartheta_0(\omega)$ overlap over a very large region in frequency space from GHz to THz. In addition, $\epsilon(\omega)$ involves slow relaxation processes below 1 GHz which are not found in $\vartheta_0(\omega)$. The overlap complicates the interpretation of experimental spectra since only the sum of these contribution can be measured.[27] The experimental data (see black triangles in Fig. 5(g)) agree reasonably with our simulations at force field density. In case of ρ_{exp}, the computational spectrum is shifted to higher frequencies (see green curve) by the acceleration factor of 2.7 discussed earlier.
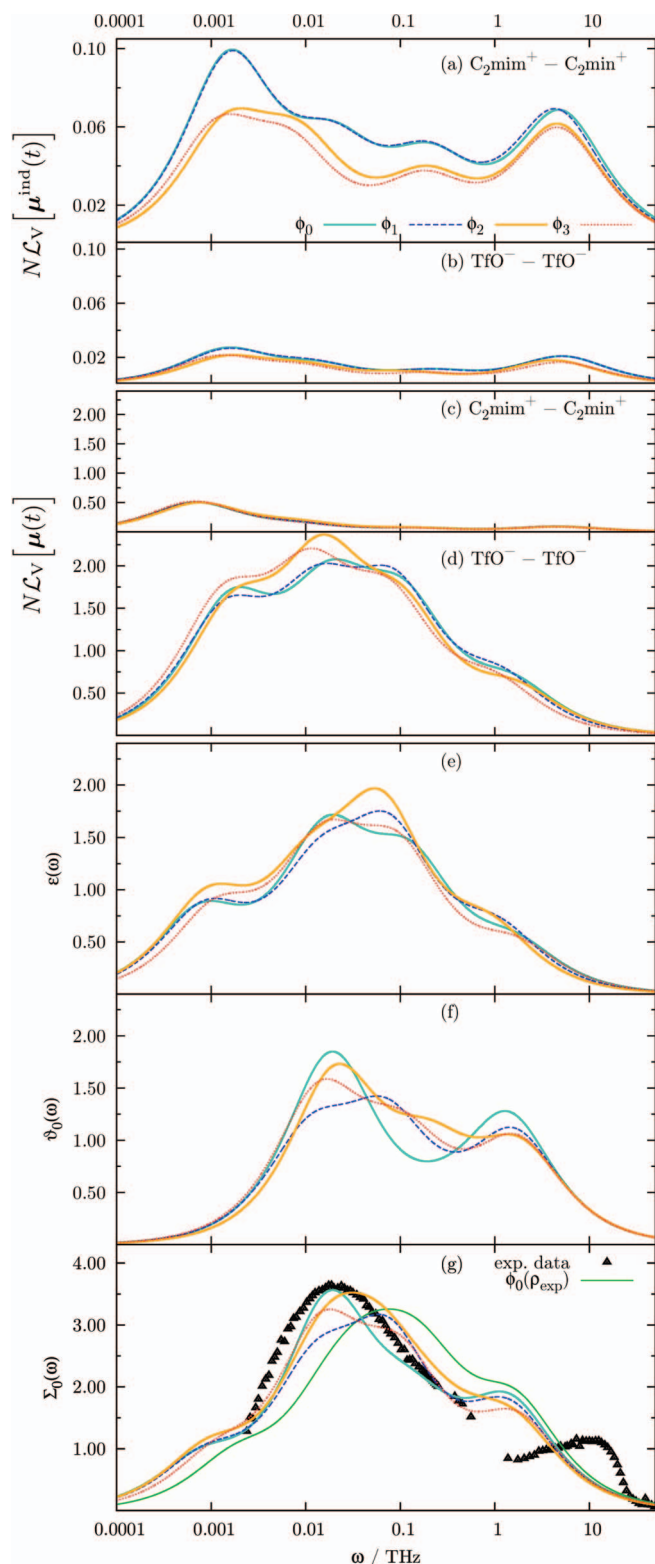
FIG. 5. Frequency-dependence of autocorrelation functions contributing to the generalized dielectric constant $\Sigma_0(\omega)$: Induced dipole moments of the cations (a) and anions (b), molecular dipole moments of cations (c) and anions (d), dielectric permittivity $\epsilon(\omega)$ (e), dielectric conductivity $\vartheta_0(\omega)$ (f), and the complete spectrum of $\Sigma_0(\omega)$ (g).

The dielectric conductivity $\vartheta_0(\omega)$ is defined by

$$\vartheta_0 = 4\pi i \frac{\sigma(\omega) - \sigma(0)}{\omega}, \qquad (14)$$

and hence depends on the conductivity $\sigma(\omega)$. Although the zero-frequency value $\sigma(0)$ at $\rho_{\exp}$ fits the experimental value of 0.774 S/m[68] better, the non-directed translational motion, $\sigma(\omega) - \sigma(0)$, is better described at the higher density ρ_{ff}. Since the $\sigma(0)$-hyperbola is commonly removed from the dielectric spectrum (cf. Eq. (14)) by experimenters and in simulations, the directed translation of charge carriers does not play a significant role in the generalized dielectric spectrum $\Sigma_0(\omega)$. In contrast, the translational contribution to $\Sigma_0(\omega)$ is dominated by the jittering of ions in the cage of their neighbors.[26]

Cage dynamics in simulations are best investigated by Voronoi tessellation.[66, 69] In particular, we have learnt that the first shell of the cage makes the essential contribution.[26] Therefore, we have calculated the mean residence time $\langle \tau_{\mathrm{cage}} \rangle$ of the cations and anions around a central ion. Here, $\langle \tau_{\mathrm{cage}} \rangle$ is the relaxation constant of the residence correlation function $\langle n(0) \cdot n(t) \rangle$, where $n(t)$ is a binary function indicating whether an ion is a member of the first shell or not.[66, 69] For a consistent interpretation we have fitted $\langle n(0) \cdot n(t) \rangle$ with a Kohlrausch-Williams-Watt function

$$\langle n(0) \cdot n(t) \rangle \simeq a \cdot e^{-\left(\frac{t}{\tau}\right)^{\beta}}. \qquad (15)$$

Thereby, β-values for the combination cation–cation (β^{++} = 0.595), cation–anion (β^{+-} = 0.748), and anion–anion (β^{--} = 0.414) could be kept fixed for all Thole functions and densities in order to reduce the number of adjustable parameters. In this way, the variation of cage migration can be mapped to a single relaxation time τ. The respective average relaxation time $\langle \tau_{\mathrm{cage}} \rangle = \tau/\beta \cdot \Gamma(1/\beta)$ is given in Table IV. Of course, the residence time $\langle \tau_{\mathrm{cage}}^{+-} \rangle$ is the longest, but neighborhood relations between like charges is only 15% shorter. This is a clear evidence of a mixed cage instead of the classical picture of an anionic cage around the cations and vice versa. This finding can also be deduced from the coordination numbers computed by $\langle n(0)^2 \rangle$:[69] C_2mim$^+$ are surrounded by 9.5 cations and 8.2 anions on average. The anionic cage consists of approximately 4.0 anions and 8.2 cations. The high number of like charge ions in the ion cage is also reported by Yan et al.[31]

Interestingly, the residence times $\langle \tau_{\mathrm{cage}} \rangle$ correlate with both, the rotational relaxation times $\langle \tau_{\mathrm{rot}} \rangle$ and diffusion coefficients, for different Thole functions ϕ_k and densities. Therefore, the cage is essential for translational migration as well as reorientation. In particular, the dynamical results from ϕ_0, ϕ_1, and ϕ_2 accompany each other but dynamics in case of ϕ_3 seems to be decelerated by at least 20%. In contrast to the structure dominated by the intramolecular region ($r < 2.5(\alpha_\beta \cdot \alpha_\gamma)^{1/6}$) in Fig. 2, the dynamics is controlled by the intermolecular zone. In fact, for $r > 2.5(\alpha_\beta \cdot \alpha_\gamma)^{1/6}$ in Fig. 2, the Thole functions ϕ_0, ϕ_1 and ϕ_2 become identical, while ϕ_3 is still below.

V. CONCLUSION

Overall, the use of Thole functions has only a moderate influence on the structure and dynamics of ionic liquids. On second sight, exponential Thole functions $\{\phi_2, \phi_3\}$ seem to reduce the molecular polarizability slightly shifting the

polarizable systems back to the non-polarizable case. Corresponding changes in structure mainly affect the distance of the ions but keep the orientation and mutual position. Changes in single-particle dynamics only occur for ϕ_3. However, this effect can be reduced significantly by enhancing the Thole radius R_3. In fact, the default value of 2.089 (cf. Table II) in AMBERis increased to 2.6 in CHARMM.[29] In any case, collective dynamics seems to be independent of Thole damping. By the way, we note that our simulations ran stable for 30 ns without any Thole function at both densities.

The different behavior of structure, single-particle, and collective dynamics can be explained by a three zone model: For very short distances below a scaled distance of 2.5, exponential Thole functions modify induced dipolar interactions in the same fashion, whereas the linear Thole function accompanies ϕ_0, i.e., no effective Thole damping. The second zone is characterized by the short intermolecular distances typical for interactions of a central ion with its cage. Here, ϕ_1 and ϕ_2 have already leveled off and behave like ϕ_0. In contrast, ϕ_3 still damps the dipolar interaction to some extent. In the third region comprising long intermolecular distances, Thole damping has leveled off. Consequently, collective dynamics is hardly affected. It is interesting to note that the principal pattern derived from the atomic $\boldsymbol{\mu}_\beta^{\text{ind}} T \boldsymbol{\mu}_\gamma^{\text{ind}}$ can be mapped on structure, single-particle, and collective dynamics of the ionic liquids molecules, respectively.

In a pictorial way our simulation studies on polarizable systems with Thole damping at various densities can be summarized by Fig. 6. Each ion is immersed in its "inner" solvent created by its induced dipoles (blue shaded areas). The interface to the inner solvent of other molecules is governed by the

Thole functions ϕ_k indicated by black dashed lines in Fig. 6. The screening by the inner solvent favors the rapprochement of like charges, thus stabilizing their residence in the cage. In fact, the cage around a central ion consists of cations and anions in comparable number. This finding strongly disagrees with the common picture of a cation surrounded solely by anions and vice versa.

Lowering the overall density results in larger distances between the like ions but hardly affects cation–anion distances. Nevertheless, these structural changes are sufficient to slacken the cage making it more permeable. This way, a central ion may escape its original cage more easily, indicated by the blue arrows in Fig. 6.
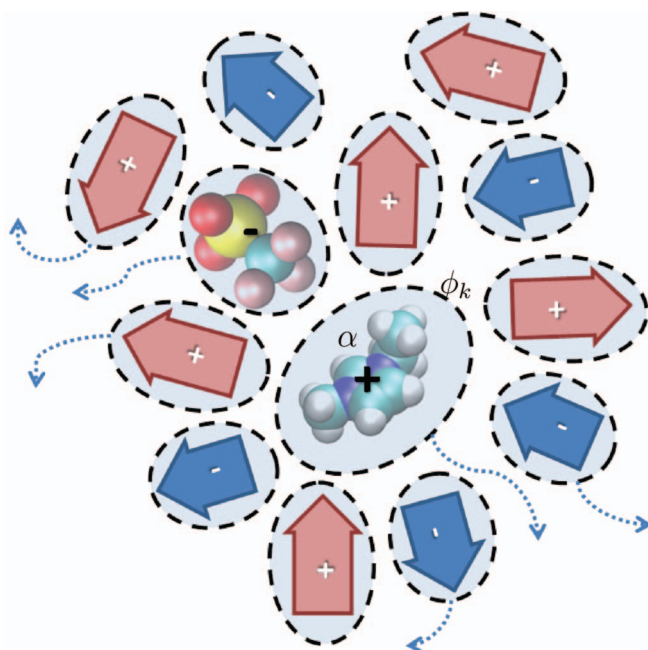
FIG. 6. The induced dipoles act as inner solvent (blue shaded areas) to damp electrostatic interaction. They are controlled by the corresponding polarizabilities α. The Thole functions ϕ_k (black dashed lines) govern the effectivity of the inner solvent at short distances. Cations and anions are displayed as red and blue arrows, respectively. The arrows indicate the direction of the corresponding dipole moments.

[1]P. A. Hunt, Mol. Simul. **32**, 1 (2006).
[2]E. J. Maginn, J. Phys.: Condens. Matter **21**, 373101 (2009).
[3]A. Triolo, O. Russina, H.-J. Bleif, and E. Di Cola, J. Phys. Chem. B **111**, 4641 (2007).
[4]O. Russina, A. Triolo, L. Gontrani, R. Caminiti, D. Xiao, L. G. Hines Jr., R. A. Bartsch, E. L. Quitevis, N. Plechkova, and K. R. Seddon, J. Phys. Condens. Matter **21**, 424121 (2009).
[5]J. N. A. Canongia Lopes and A. A. H. Pádua, J. Phys. Chem. B **110**, 3330 (2006).
[6]A. A. H. Pádua, M. F. Costa Gomes, and J. N. A. Canongia Lopes, Acc. Chem. Res. **40**, 1087 (2007).
[7]Y. Wang, W. Jiang, T. Yan, and G. A. Voth, Acc. Chem. Res. **40**, 1193 (2007).
[8]S. M. Urahata and M. C. C. Ribeiro, J. Chem. Phys. **120**, 1855 (2004).
[9]J. N. Canongia Lopes, J. Deschamps, and A. A. H. Pádua, J. Phys. Chem. B **108**, 2038 (2004).
[10]J. N. Canongia Lopes and A. A. H. Pádua, J. Phys. Chem. B **108**, 16893 (2004).
[11]T. Yan, C. J. Burnham, M. G. Del Pópolo, and G. A. Voth, J. Phys. Chem. B **108**, 11877 (2004).
[12]A. Bagno, F. D'Amico, and G. Saielli, J. Mol. Liq. **131–132**, 17 (2007).
[13]L. J. A. Siqueira and M. C. C. Ribeiro, J. Phys. Chem. B **111**, 11776 (2007).
[14]J. Pićalek and J. Kolafa, J. Mol. Liq. **134**, 29 (2007).
[15]E. J. Maginn, Acc. Chem. Res. **40**, 1200 (2007).
[16]C. Schröder and O. Steinhauser, J. Chem. Phys. **133**, 154511 (2010).
[17]F. Dommert, J. Schmidt, C. Krekeler, Y. Y. Zhao, R. Berger, L. delle Site, and C. Holm, J. Mol. Liq. **152**, 2 (2010).
[18]V. V. Chaban, I. V. Voroshylova, and O. N. Kalugin, Phys. Chem. Chem. Phys. **13**, 7910 (2011).
[19]B. L. Bhargava and S. Balasubramanian, J. Chem. Phys. **127**, 114510 (2007).
[20]W. Zhao, H. Eslami, W. L. Cavalcanti, and F. Müller-Plathe, Z. Phys. Chem. **221**, 1647 (2007).
[21]J. Schmidt, C. Krekeler, F. Dommert, Y. Zhao, R. Berger, L. delle Site, and C. Holm, J. Phys. Chem. B **114**, 6150 (2010).
[22]D. Roy and M. Maroncelli, J. Phys. Chem. B **114**, 12629 (2010).
[23]D. T. Bowron, C. D'Agostino, L. F. Gladden, C. Hardacre, J. D. Holbrey, M. C. Lagunas, J. McGregor, M. D. Mantle, C. L. Mullan, and T. G. A. Youngs, J. Phys. Chem. B **114**, 7760 (2010).
[24]M. Kohagen, M. Brehm, J. Thar, W. Zhao, F. Müller-Plathe, and B. Kirchner, J. Phys. Chem. B **115**, 693 (2011).
[25]H. Liu and E. Maginn, J. Chem. Phys. **135**, 124507 (2011).
[26]C. Schröder, J. Chem. Phys. **135**, 024502 (2011).

[27]C. Schröder, T. Sonnleitner, R. Buchner, and O. Steinhauser, Phys. Chem. Chem. Phys. **13**, 12240 (2011).

[28]C. Schröder, Phys. Chem. Chem. Phys. **14**, 3089 (2012).

[29]B. R. Brooks, C. L. Brooks III, A. D. Mackerell, L. Nilsson, R. J. Petrella, B. Roux, Y. Won, G. Archontis, C. Bartels, S. Boresch, A. Caflisch, L. Caves, Q. Cui, A. R. Dinner, M. Feig, S. Fischer, J. Gao, M. Hodoscek, W. Im, K. Kuczera, T. Lazaridis, J. Ma, V. Ovchinnikov, E. Paci, R. W. Pastor, C. B. Post, J. Z. Pu, M. Schaefer, B. Tidor, R. M. Venable, H. L. Woodcock, X. Wu, W. Yang, D. M. York, and M. Karplus, J. Comput. Chem. **30**, 1545 (2009).

[30]W. Jiang, T. Yan, Y. Wang, and G. A. Voth, J. Phys. Chem. B **112**, 3121 (2008).

[31]T. Yan, Y. Wang, and C. Knox, J. Phys. Chem. B **114**, 6886 (2010).

[32]T. Yan, Y. Wang, and C. Knox, J. Phys. Chem. B **114**, 6905 (2010).

[33]I. T. Todorov, W. Smith, K. Trachenko, and M. T. Dove, J. Mater. Chem. **16**, 1911 (2006).

[34]T.-M. Chang and L. X. Dang, J. Phys. Chem. A **113**, 2127 (2009).

[35]O. Borodin, J. Phys. Chem. B **113**, 11463 (2009).

[36]O. Borodin, W. Gorecki, G. D. Smith, and M. Armand, J. Phys. Chem. B **114**, 6786 (2010).

[37]J. B. Hooper, O. N. Starovoytov, O. Borodin, D. Bedrov, and G. D. Smith, J. Chem. Phys. **136**, 194506 (2012).

[38]See www.wasatchmolecular.com/WMI-MD_product.html (last access May 2013).

[39]AMBER, Assisted model building with energy refinement, 2012 see http://www.ambermd.org/.

[40]M. G. Del Pópolo, R. M. Lynden-Bell, and J. Kohanoff, J. Phys. Chem. B **109**, 5895 (2005).

[41]C. Spickermann, J. Thar, S. B. C. Lehmann, S. Zahn, J. Hunger, R. Buchner, P. A. Hunt, T. Welton, and B. Kirchner, J. Chem. Phys. **129**, 104505 (2008).

[42]S. Zahn, J. Thar, and B. Kirchner, J. Chem. Phys. **132**, 124506 (2010).

[43]M. Brüssel, M. Brehm, T. Voigt, and B. Kirchner, Phys. Chem. Chem. Phys. **13**, 13617 (2011).

[44]S. Gabl, C. Schröder, and O. Steinhauser, J. Chem. Phys. **137**, 094501 (2012).

[45]H. Yu and W. F. van Gunsteren, Comput. Phys. Commun. **172**, 69 (2005).

[46]S. W. Rick, S. J. Stuart, and B. J. Berne, J. Chem. Phys. **101**, 6141 (1994).

[47]S. Patel and C. L. Brooks III, J. Comput. Chem. **25**, 1 (2004).

[48]M. C. C. Ribeiro, Phys. Rev. B **63**, 094205 (2001).

[49]G. Lamoureux and B. Roux, J. Chem. Phys. **119**, 3025 (2003).

[50]H. Yu, T. Hansson, and W. F. van Gunsteren, J. Chem. Phys. **118**, 221 (2003).

[51]E. Harder, V. M. Anisimov, I. V. Vorobyov, P. E. M. Lopes, S. Y. Noskov, A. D. MacKerell Jr., and B. Roux, J. Chem. Theory Comput. **2**, 1587 (2006).

[52]D. P. Geerke and W. F. van Gunsteren, J. Chem. Theory Comput. **3**, 2128 (2007).

[53]D. van der Spoel, E. Lindahl, B. Hess, G. Groenhof, A. E. Mark, and H. J. C. Berendsen, J. Comput. Chem. **26**, 1701 (2005).

[54]B. T. Thole, Chem. Phys. **59**, 341 (1981).

[55]P. T. van Duijnen and M. Swart, J. Phys. Chem. A **102**, 2399 (1998).

[56]J. Applequist, J. R. Carl, and K.-K. Fung, J. Am. Chem. Soc. **94**, 2952 (1972).

[57]Y. Gu and T. Yan, J. Phys. Chem. A **117**, 219 (2013).

[58]J. Applequist, Accounts Chem. Res. **10**, 79 (1977).

[59]H. Rodriguez and J. F. Brennecke, J. Chem. Eng. Data **51**, 2145 (2006).

[60]H. De Loof, L. Nilsson, and R. Rigler, J. Am. Chem. Soc. **114**, 4028 (1992).

[61]K. Bica, C. Schröder, M. Deetlefs, and K. R. Seddon, Phys. Chem. Chem. Phys. **15**, 2703 (2013).

[62]P. A. Madden and M. Wilson, Chem. Soc. Rev. **25**, 339 (1996).

[63]C. Schröder, T. Rudas, and O. Steinhauser, J. Chem. Phys. **125**, 244506 (2006).

[64]J. M. Crosthwaite, M. J. Muldoon, S. N. V. K. Aki, E. J. Maginn, and J. F. Brennecke, J. Phys. Chem. B **110**, 9354 (2006).

[65]W. L. Jorgensen, D. S. Maxwell, and J. Tirado-Rives, J. Am. Chem. Soc. **118**, 11225 (1996).

[66]C. Schröder, G. Neumayr, and O. Steinhauser, J. Chem. Phys. **130**, 194503 (2009).

[67]C. Schröder and O. Steinhauser, J. Chem. Phys. **131**, 114504 (2009).

[68]N. Ignat'ev, U. Welz-Biermann, A. Kucheryna, G. Bissky, and H. Willner, J. Fluorine Chem. **126**, 1150 (2005).

[69]G. Neumayr, C. Schröder, and O. Steinhauser, J. Chem. Phys. **131**, 174509 (2009).